NUMERICAL FATIGUE LIFE ANALYSIS OF COMBUSTION CHAMBER WALLS FOR FUTURE REUSABLE LIQUID ROCKET ENGINES (LREs) APPLICATIONS

SPACE PROPULSION 2022
ESTORIL, PORTUGAL | 09 – 13 MAY 2022

Mateusz T. Gulczyński [1,2], Jörg R. Riccius [1], Günther Waxenegger-Wilfing [1], Jan C. Deeken [1], Michael Oschwald [1,2]

[1] German Aerospace Research Center DLR Lampoldshausen, Germany
[2] RWTH Aachen University, Germany
Mateusz.Gulczynski@dlr.de, Michael.Oschwald@dlr.de, Joerg.Riccius@dlr.de, Guenther.Waxenegger@dlr.de, Jan.Deeken@dlr.de

KEYWORDS: ANSYS Parametric Design Language (APDL), combustion chamber (CC), damage propagation, doghouse effect, low cycle fatigue (LCF), liquid rocket engines (LREs), PROMETHEUS, reusable launch vehicles (RLVs), thermo-mechanical fatigue (TMF)

ABSTRACT:

Within the presented manuscript the focus is towards maturing damage propagation simulation models of the regeneratively cooled combustion chamber (CC) inner liner, to gain an in-depth understanding of the interactions between influential elements including elevated temperature, cyclic conditions and the fatigue life mechanisms. A coupled thermal and structural 2D Finite Element Analysis (FEA) of a CC wall nozzle throat cross-section was set-up comprising the full cycle with pre-cooling, start-up, hot run, post-cooling and relaxation back to ambient temperature and pressure. The remaining useful life of the CC wall was estimated by a post-processing method including the cumulative effect of the fatigue damage and tensile strain accumulation. The proposed accumulative damage model for the low cycle fatigue (LCF) analysis consists of a model's combination in accordance with Bonora-Gentile-Pirondi (2004) and Dufailly-Lemaitre (1995). Contrary to conventionally proposed studies with damage parameter values integrated as state variables in the FEA, we propose an alternative approach by introducing the damage parameter in the post processing method to save numerical analysis time. The integration of a directional progressive accumulation of plastic strain in cyclic thermo-mechanical loading, is especially important for rocket engine components during their test phase, as well as to increase the reusability capacity of the future reusable launch vehicles (RLVs).

1. INTRODUCTION

The development of reusable liquid rocket engines (LREs), with reusability capacity of minimum 10 missions [1], requires introduction of well-structured methods for the evaluation of the critical sub-components' remaining useful life. The regeneratively cooled combustion chamber (CC) inner liner is subjected to an extremely high load – mainly resulting from the large temperature gradient between the hot gas and the low temperature of the coolant. Repeated loading and unloading operations combined with effects such as high temperature and viscoplastic strain, reduce considerably the life of the combustion chamber inner liner [2].
In Figure 1, the cryogenic Methane/Oxygen (LCH4/LOX) powered "Prometheus" engine is shown – the main stage of the European Ariane 6 (to replace the Vulcain 2 engine currently powering Ariane 5), both regeneratively cooled and based on the gas generator engine cycle. Within a nominal combustion chamber pressure of 10 MPa, the peak heat load in the nozzle throat area is larger than 80[MW/m^2] [3]. This results in a large radial temperature gradient in the combustion chamber wall, leading to an immense heat flux and thermal stresses, emerging the failure in the inner liner (Figure 1 A-A c.s.- LCF crack microscopic view). The presented cross-section of the CC cooling channels with a microscopic view of a Thermo-Mechanical Fatigue (TMF) cut-out, was tested to failure at the DLR Lampoldshausen laboratory test bench M51. At M51, nozzle structures experiments are conducted for validation purposes of nozzle life prediction models, including combustion chamber thermomechanical analyses. A more detailed description of the test bench may be found at [4], [5]. The TMF facility (Figure 2) provides essential validation data for numerical analyses and may support the full-scale tests of CC.

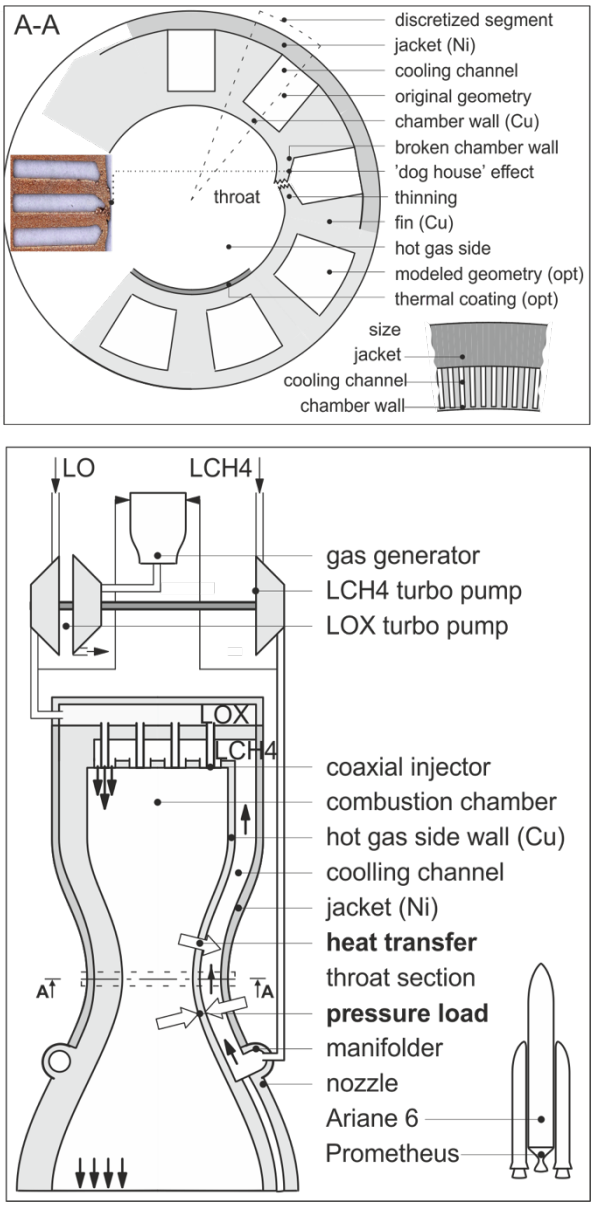

Figure 1. Gas generator engine schematic with a regeneratively cooled combustion chamber cross-section (A-A) and a middle cross section of the TMF panel with visible "dog house" effect- LCF crack - microscopic view (left-hand side of the A-A)

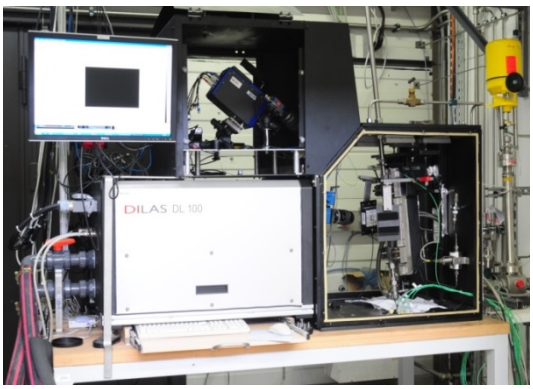

Figure 2 Thermo-Mechanical Fatigue (TMF) laboratory test set-up at DLR Lampoldshausen used for validation of the FE analysis results. Left-hand side – laser head, top – infra-red camera, right-hand side – TMF panel housing.

Within this manuscript, we evaluate the following aspects for an efficient numerical fatigue life analysis of the combustion chamber for future reusable LRE's applications:

- In (**Section 2**), the motivation of the research for future reusable LREs is explained, highlighting the product life cycle, the main requirements imposed on fracture critical structures, such as CC, and a general approach towards efficient evaluation of the CC's fatigue life;

- (**Section 3 and 4**) are focused on explaining a methodology for calculating the remaining useful life of the CC inner liner with an overview of the proposed FE plasticity model as well as post-processing accumulative damage model for the low cycle fatigue (LCF) analysis in accordance with Bonora-Gentile-Pirondi (2004) and Dufailly-Lemaitre (1995). The description of applied methodology is followed by a more comprehensive presentation of the applied constitutive model;

- The Finite Element model developed for CC evaluation is presented in (**Section 5**). A one way-coupled thermal and structural 2D FEA of the CC's wall nozzle throat cross-section model is described including a definition of applied boundary conditions, laser loading sequence as well as a temperature profile;

- In (**Section 6**) the methodology and results of the applied post-processing method for the ductile and brittle damage components calculation is shown. A comparison of two applied methods is presented: one, where the post-processing method is based on the data from FE simulation with all cycles to failure, and an alternative method, allowing even faster estimation of the fatigue life, where the post-processing analysis is based on the initial two numerically acquired FE cycles. The critical number of cycles to failure with a failure position in the CC is shown;

- Finally, in the concluding (**Section 7**), the post-processing results are compared against the validation data from the laboratory experiments. The comparison of the CC type TMF panel cross section, where a deformation of the cooling channels is visible (from the TMF panel test bench DLR Lampoldshausen) and numerically obtained cross-section, highlighting a total mechanical strain in X-direction, is presented.

2. MOTIVATION AND GENERAL APPROACH

The requirements imposed on the fracture of critical structures such as LREs combustion chambers – exposed to the severe thermomechanical loads [2], [6], [7] as well as increased operational and production costs associated with RLV technology development and flight qualification requirements, motivates the research towards solutions with more efficient numerical models where the computational time can be considerably reduced and given engine conditions could be quickly evaluated. For a reusable engine the time dependent model incorporating specific mission profiles includes the following cycle events: acceptance test (3-4 cycles 215- 890[s]), ascent phase (estimated 1 cycle, 100-130[s]) and retro propulsion manoeuvres (estimated 3 cycles, 30[s]). Based on the literature review, it could be concluded that for – the reusable unit – the engine would have to withstand at least 43 cycles assuming 10 flight missions (Table 1) [8], [9].

	Product Life Cycle Event		Duration* [s]	No. of cycles*
Acceptance Test	Single MLC (Main Life Cycle) incl. hot fire test	Acceptance hot-fire test before the actual flight; Engine ground start hold-down with launch commit criteria abort; A single flight mission duration + several flight missions for reusable main stage engine;	215 →890	3→4
Ascent Phase	Lift-Off	Vertical take-off	0.2 →0.1	1
	Pitch Over	Constant pitch rate	11.8 →4.1	
	Pitch Constant	Transition to gravity turn	6 →3.3	
	Gravity turn	Angle of attack is zero	47 →42.5	
	Ascent	With stage separation	130 →100.2	
	Mission nominal time		165 →520	
Retro Propulsion Man.	Flip Over and Boost Back Burn Manoeuvre	Nitrogen thrusters used for flip over; ignition of 3 of 9 main engines (Falcon9 case);	≅ 30	3
	Re-entry burn	Re-ignition of three engines- ballistic re-entry		
	Touch down	Central engine is re-ignited shortly before landing		

Table 1 Product life cycle for reusable LRE

* this could vary in dependence on the engine type

Within each hot-fire operation, there is a degradation of the components by two underlying failure mechanisms of cyclic strain-increase and time dependable strength-reduction. Consequently, the components are subjected to failure modes of wear, erosion, creep, fatigue (with crack initiation and propagation) as well as a failure by thermal ageing [7], [8]. The most frequently encountered fatigue failures modes of thrust chambers of LRE's RLV applications are:
(I) LCF resulting from a cyclic plastic deformation of the inner wall in the course of repeated operations;
(II) creep of the inner wall (high temperature rate dependent inelastic strain);
(III) thermal ratcheting (occurring due to a combination of cyclic thermal stress (secondary stress) superimposed on constant load controlled stress (primary stress) [10]).
A deformation increases progressively accumulating in the load-controlled stress direction applied as the number of cycles of the thermal stress grows [11]. This results in a cyclic accumulation of plastic strain in the inner wall. In the case of the double- wall thrust chamber (inner liner and outer jacket), the primary mode of failure is by bending, "dog house effect" (ratchetting and bulging into the hot gas) and rupture of the inner wall ligament [12].

To evaluate the remaining useful life of the CC wall, a damage accumulation method is introduced, where the damage variables are obtained through a combination of the two models in accordance with Bonora-Gentile-Pirondi (2004) for ductile failure and Dufailly-Lemaitre (1995) for brittle failure. The damage accumulation is a result of the loading parameters, such as the stress ratio, the mean stress and the loading sequence. The accumulated plastic strain approach (including both: the ductile and the brittle damage part) is applicable for LCF, but not for HCF. The advantage of the model is mainly due to the post processing implementation of various fatigue life analysis methods. This results in a combined model (taking into account both, ductile damage and classical fatigue failure). The failure is related to both, the total mechanical strain (ductile damage) + and the accumulated plastic strain (brittle damage + macro propagation part). In opposition to the originally proposed method, where damage parameter values are integrated as a state variable in the FEA, we present an alternative approach by incorporating the damage parameter in the post processing stage to save numerical analysis time. Furthermore, to considerably reduce the analysis time, the calculation of the component's remaining useful life is further based on the initial two numerically acquired cycles. Following the numerical analysis, a critical damage of the CC is derived in the post-processing step. The integration of a progressive accumulation of plastic strain in the course of cycling stress – is especially important for rocket engine components during their test phase, as well as to increase the reusability capacity of the future RLVs. Finally, the outcome of the FE and the post-processing analyses are validated with the TMF laboratory results acquired at M51 side.

3. FINITE ELEMENT PLASTICTY MODEL

To predict the nonlinear behavior of the CC liner material (CuCrZr), where an increased number of cycles are expected, the coupling between plasticity models and damage is crucial. Within presented model a damage isotropy (where microcarcaks and microviods are uniformly distributed in all directions) is assumed as a sufficient simplification to achieve a reliable result and to evaluate the CC's critical number of cycles to failure.

A continuum, plasticity-based model is applied to represent the elasto-plastic deformation of a CC. The inner liner of this CC is assumed to be made from the high-conductivity copper-based alloy CuCrZr. This material is composed of chromium (preventing an extensive grain growth during the recrystallization process at increased temperature) and zirconium particles. Zirconium refines the grains and ties the oxygen within the structure. The yield surface evolution is controlled by the main hardening variable: plastic strain "ε^{pl}".

The elasto-plastic constitutive theory implemented to the model and presented in this section focuses on evaluating the influence of irreversible damage corresponding to failure mechanisms that are observed in the CC structure materials under thermal and pressure loading conditions [13]. An elasto-plastic model is used where the deformation is divided into its elastic, plastic and thermal part:

$$\dot{\varepsilon} = \dot{\varepsilon}^{e} + \dot{\varepsilon}^{p} + \dot{\varepsilon}^{th} \qquad \text{Eq. 1}$$

(strain rate decomposition), which relates the objective stress rate to the elastic part of the deformation by:

$$\dot{\sigma} = C^{\sigma J} : (\dot{\varepsilon} - \dot{\varepsilon}^{p} - \dot{\varepsilon}^{th}) \qquad \text{Eq. 2}$$

A damage-caused reduction of the elastic stiffness is not taken into account for the Finite Element analyses, presented in this manuscript. Formulas applied for the FE analysis are shown in *Table 2*.

Nomenclature	**PARAM**	**Calculation Formula**	**Unit**	**Eq. Nr.**
Hydrostatic stresses	σ_H	$= \frac{\sigma_{11}+\sigma_{22}+\sigma_{33}}{3} = \frac{1}{3}tr(\sigma) = \frac{1}{3}I_1 = \frac{1}{3}\sigma_{kk}$	MPa	(3)
Von Mises equivalent stress	σ_{eq}	$= \sqrt{\frac{3}{2}\sigma_{ij}^{D}\sigma_{ij}^{D}}$	MPa	(4)
Stress deviator	σ_{ij}^{D}	$= \sigma_{ij} - \frac{1}{3}\sigma_{kk}\delta_{ij}$	MPa	(5)
Effective accumulated plastic strain rate ($\dot{p}_{(t)}$)	$\dot{p}$	$= \sqrt{\frac{2}{3}\dot{\varepsilon}_{ij}^{p}\dot{\varepsilon}_{ij}^{p}}\,;\ \dot{p} = (\frac{f}{K})^{N}$	-	(6)
Strain hardening power law for 1-D case	ϵ_p	$= (\frac{\sigma - \sigma_y}{K})^{N}$ * "K" and "N" identified from tensile test curve		

Table 2. Formulas used for Finite Element analysis

4. POST-PROCESSING FATIGUE LIFE ANALYSIS

The damage evolution is highly dependable on the selected damage potential, what directly influence the damage "response" – resulting in damage increase progressing faster or slower with respect to deformation [14]. This is especially evident for ductile materials, where the damage potential must be properly designed, correspondingly to the experiment conditions as well as obtained laboratory results.

Within the presented post-processing fatigue life analysis approach, a combination of ductile and brittle damage models is introduced. In both models, damage "*D*" is related to the decrease of the elasticity modulus "$\acute{E}$" induced by the damage:

$$D = 1 - \frac{A_{\text{eff}}}{A_0} = 1 - \frac{E_{\text{eff}}}{E_0} \qquad \text{Eq. 7}$$

where "E_0" and "E_{eff}" are the Young's modulus of the undamaged and damaged materials respectively and "*D*" is damage variable [15]. Therefore, for uniaxial tests, the damage "*D*" may be measured by means of the decrease of the effective Young´s modulus resulting from the softening process induced by the damage.

This definition is based on the assumption, that the damage variable is given as the ratio of the damaged reference volume area "A_D=1-A_{eff}" to the nominal one. The variable "A_D" accounts for voids and microcracks which reduce the reference volume element (RVE) effective net resisting area and their mutual interactions. The damage variable is expressed as the material stiffness reduction (based on the effective stress definition). The stress-based definition of damage has a following form:

$$D = 1 - \frac{\sigma_s}{\sigma_u} \qquad \text{Eq. 8}$$

where "σ_s"– actual yield stress, "σ_u"– ultimate stress.

As explained in the following sections, the calculated accumulative damage model for the LCF evaluation, comprise a combination of models in accordance with Bonora-Gentile-Pirondi (2004) and Dufailly-Lemaitre (1995). The calculated variables are applied over numerous load cycles to project the probability of the crack initiation and for the faster fatigue life evaluation of the CC component. Furthermore, the presented methodology is further applied to allow for even faster estimation of the remaining useful life of the CC, by extrapolation of the acquired data (methodology explained thoroughly in section 6).

Ductile Damage model based on Bonora (2004)

In accordance with Bonora, the damage rate can be calculated as:

$$\dot{D} = \alpha \left[\frac{D_{\mathrm{cr}} - D_0}{\ln(\varepsilon_{\mathrm{f}}/\varepsilon_{\mathrm{th}})}\right] f\left(\frac{\sigma_{\mathrm{m}}}{\sigma_{\mathrm{eq}}}\right) (D_{\mathrm{cr}} - D)^{(\alpha-1)/\alpha} \frac{\dot{p}}{p} \quad \text{Eq. 9}$$

Under the assumption of proportional loading "$f(\sigma_{\mathrm{m}}/\sigma_{\mathrm{eq}}) = \text{constant}$" this equation can be written in the following form:

$$D = D_0 + (D_{cr} - D_0)\left\{1 - \left[1 - \frac{\ln(p/p_{th})}{\ln(\varepsilon_f/\varepsilon_{\mathrm{th}})} f\left(\frac{\sigma_{\mathrm{m}}}{\sigma_{eq}}\right)\right]^{\alpha}\right\} \quad \text{Eq. 10}$$

In case of a uniaxial loading condition "$\mathrm{TF} = 0.333$" and "$f(\sigma_{\mathrm{m}}/\sigma_{\mathrm{eq}}) = 1.0$", may take further form of:

$$D = D_0 + (D_{cr} - D_0)\left\{1 - \left[1 - \frac{\ln(\varepsilon/\varepsilon_{\mathrm{th}})}{\ln(\varepsilon_{\mathrm{f}}/\varepsilon_{\mathrm{th}})}\right]^{\alpha}\right\}) \quad \text{Eq. 11}$$

The damage variable equation (Eq. 7) constitutes a definition for the damage, as it is possible to monitor the variation of the initial stiffness during strain accumulation in a tensile test executing partial unloading at given strain levels [15]. All required parameters that include: damage threshold strain "ε_{th}", uniaxial strain to failure "ε_f", critical damage "D_{cr}", damage evolution exponent "α", initial damage "D_0" (where "D_0" may be assumed to be 0 in case of the virgin material) must be known/identified in advance [15].

The example of damage evolution in function of strain for a given damage parameter set and a damage parameter exponent, is shown in Figure 3. The more detailed description of the damage evolution exponent influence in the frame of the presented research, will be explained in the following section 6.

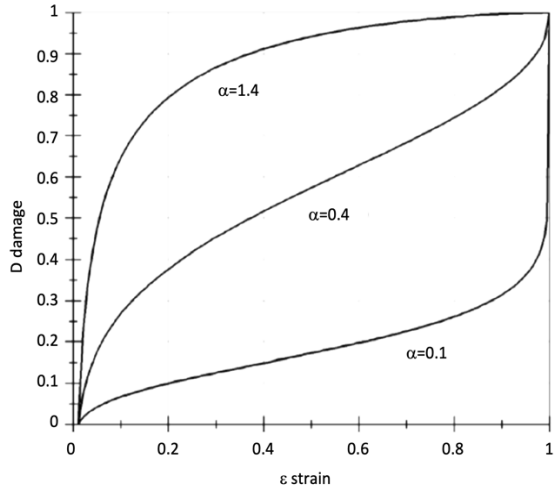

Figure 3 Example of different damage evolutions vs strain for a given damage parameter set (ε_{th} =0.01, ε_f =1.0, D_{cr} =1.0) and different choices of the α exponent (adapted from [16])

Brittle fatigue damage model based on Lemaitre-Desmorat and Dufailly-Lemaitre (1995)

In accordance with Dufailly and Lemaitre, the evolution of damage may be calculated as:

$$\dot{D} = \left(\frac{\sigma_{eq}^2 R_v}{2ES(1-D)^2}\right)^s \dot{p} \quad \text{Eq. 12}$$

where "R_v" is the following triaxiality function:

$$R_v = f\left(\frac{\sigma_{\mathrm{m}}}{\sigma_{\mathrm{eq}}}\right) = \frac{2}{3}(1+\nu) + 3(1-2\nu)\left(\frac{\sigma_{\mathrm{m}}}{\sigma_{\mathrm{eq}}}\right)^2 \quad \text{Eq. 13}$$

Equation (12) may be integrated if "*D<1*" to determine the condition of the crack initiation at a Very Low Cycle Fatigue (VLCF) process, when "σ_{eq}", "σ_H", "σ_m " and "p" are known [17]. To find out the conditions of the crack initiation, the differential constitutive equation as a post processing approach of a structural FE analysis may be used. The acquired data of the accumulated plastic strain rate "$\dot{p}_{(t)}$", the equivalent stress "σ_{eq}" and the hydrostatic stress "σ_H" must be extracted from the results of the Finite Element analysis. Moreover, the material parameters at a given temperature must be experimentally identified, that includes: "σ_s" (plastic threshold), "*E*", "*S*", "*s*" (exponent determined from fracture conditions). The parameters are to be determined from a strain controlled tension-compression test, at constant amplitude of strain.

The complete set of calculation formulas for estimating the critical number of cycles to failure of the CC's inner liner are presented in Table 3.

Nomenclature	**PARAM**	**Calculation Formula**	**Unit**	**Eq. Nr.**
Decrease of elastic modulus $\tilde{E}$ induced by the damage (IAW Lemaitre)	D D_c	$= 1 - \frac{\tilde{E}}{E}$ $= 1 - \frac{\sigma_{r(upture\ engineering\ stress)}}{\sigma_{u(niaxial\ max\ stress)}}$	-	(14)
Damage evolution for the uniaxial loading case R_v=1;(IAW Bonora)	D_{du}	$= D_{cr}\{1 - [1 - \frac{\ln\left(\frac{\varepsilon}{\varepsilon_{th}}\right)}{\ln\left(\frac{\varepsilon_f}{\varepsilon_{th}}\right)}]^{\alpha}\}$		(15)
Triaxiality function	R_v	$= \frac{2}{3}(1+\nu) + 3(1-2\nu)(\frac{\sigma_H}{\sigma_{eq}})^2$		(16)
Kinetic damage or periodic loading (IAW Lemaitre)	$\dot{D}$	$= \left(\frac{\sigma_{eq}^2 R_v}{2ES(1-D)^2}\right)^s \dot{p}$	-	(17)
Kinetic damage evolution law (IAW Bonora)	$\dot{D}$	$= \alpha \frac{(D_{cr} - D_0)^{\frac{1}{\alpha}}}{\ln\left(\frac{\varepsilon_f}{\varepsilon_{th}}\right)} R_v (D_{cr} - D)^{\frac{\alpha-1}{\alpha}} \frac{\dot{p}}{p}$		(18)

Table 3. Calculation formulas for damage and critical fatigue life evaluation

5. FINITE ELEMENT DISCRETIZATION

The CC's structural FEM model (Figure 4), represents the core section of the TMF panel tested at the DLR Lampoldshausen laboratory site. The dimensions of the cooling channels and the thin area are analogous to Prometheus engine's CC. A structural evaluation is based on the theoretical model and variables highlighted in Table 4 and Table 5, including viscosity parameters, acquired during the laboratory tests of the CuCrZr material. The hardening parameters are identified through the cyclic tension/compression test optimized by means of the least-square method. The model is meshed with 4782 "Solid185" elements (eight nodes having three degrees of freedom at each node). The boundary conditions are applied on the area on the face normal to the X direction, and the inlet surface is fixed in the transverse direction of the cooling channels. The coupling is implemented to allow for the same nodal temperature and pressure displacement in the X, Z nodal direction.

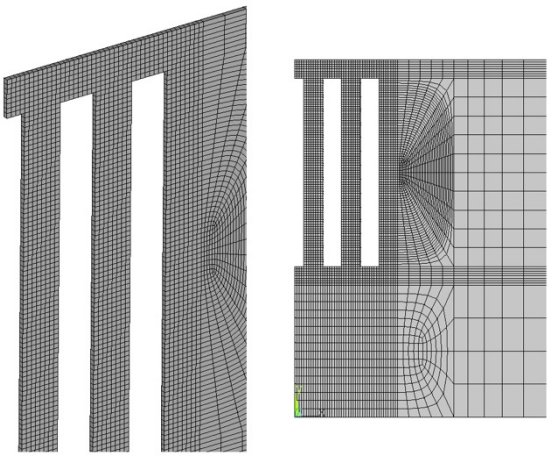

Figure 4. Mesh of the quasi-2-D model. One element in the Z direction. A total of 4782 8-node 3d elements used.

A coupled thermal and structural 2D FEA of the CC's wall nozzle throat cross-section was set-up comprising the full cycle including: pre- cooling, hot run (laser loading phase), and post cooling. The laser loading sequence is shown in Figure 5. The laser beam profile (*Figure 6*) was used in the FEM simulation to represent the real conditions applied as a heat flux of 20[MW/m^2] in the thickness direction (Y direction) of the CC type TMF panel model. The coolant (N_2) mass flow rate was adjusted to obtain the tested temperature of 900[K] (*Figure 7*). The applied coolant temperature of 160[K] is a result of mixing cryogenic and ambient temperature Nitrogen. The pressure inside the cooling channels of ≈5[MPa] was applied on the cooling channels surface to simulate the coolant (Nitrogen) which, for safety reasons, was used as replacement of CH_4 [4], [18], [19], [20], [21].

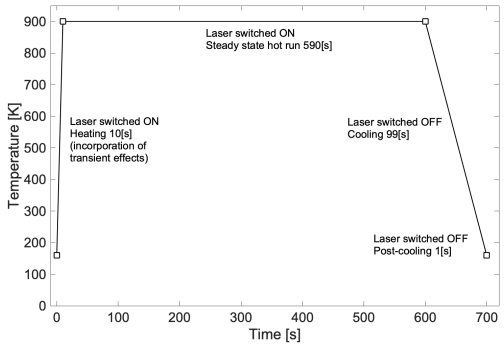

Figure 5 Time dependency of the maximum TMF panel temperature, caused by laser loading for each fatigue-relevant cycle (T_{max}=900[K])

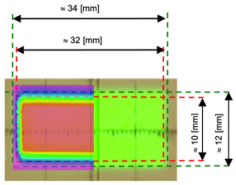

Figure 6 Laser beam intensity distribution at the focal plane, determined with a beam profiler (left) and visualized with an infra-red conversion screen for the Q=20[MW/m^2] optics

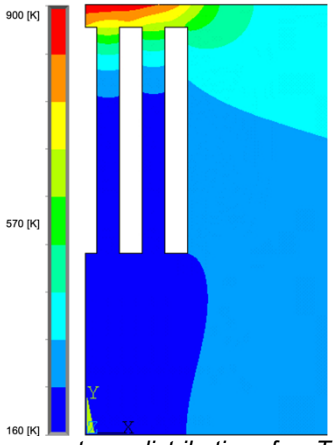

Figure 7 Temperature distribution for T_{max}= 900[K], $T_{coolant}$= 160[K] resulting from the thermal FE analysis

The material parameters (Table 4) were least-squares fitted from the results of uni-axial tests with the TMF panel material and used mainly for the FE analysis ("E" and "ν" also applied in the post processing). The numerically obtained results, applied to the post-processing analysis, include: time, stresses (incl. hydrostatic stress), elastic and plastic strains, Von Mises and equivalent plastic strains, plastic strain rate, local temperature.

Nomenclature	**Parameter**	**Unit**	**T= 300[K]**	**T= 700[K]**	**T= 900[K]**
Young's modulus	E	MPa	115680	113750	95100
Poisson's ratio	ν	-	0.3	0.3	0.3
Viscosity parameters	K	MPa	570	3050	365
	N	-	5.5	1.8	4.5
Yield stress	σ_s (or σ_y)	MPa	160.5	142.9	31.8
	R_∞	MPa	55	-10	-18
	R_0	MPa	-0.1	-5.0	-3.0
Kinematic hardening parameters	X_∞	MPa	60.3	64.2	19.2
	γ	-	300	700.8	620.6

Table 4 Structural material parameters least-squares-fitted from the isothermal fatigue (LCF) and tensile tests as used for the FE analysis

6. POST-PROCESSING ANALYSIS

The damage evolution is expressed with the following generalized model:

$$D_{total} = D_{ductile} + D_{brittle} \quad \text{Eq. 19}$$

where "D_{total}" represents the combined ductile and brittle damage (equation written in its incremental form).
To implement the damage evolution equation in the post processing step and evaluate the crack initiation, material parameters "σ_s", "E", "S", "s", must be experimentally acquired. For the presented research a least-squares fitted from of the results from uni-axial tension-compression LCF tests were implemented. The basic parameters obtained from the uni-axial material tests and used for the post processing CC's fatigue life evaluation are shown in Table 5.

Nomenclature	Parameter	Unit	T= 300[K]	T= 700[K]	T= 900[K]
Critical damage value at tensile test	D_{cr}	-	0.50	0.38	0.62
Theoretical strain to failure that a ductile material would exhibit under uniaxial stress	ε_f	-	0.24	0.24	0.16
Damage threshold strain	ε_D (or ε_{th})	-	0.002	0.002	0.0008
Damage exponent	α	-	0.4	0.46	0.14
Material fitting parameter	S_1 (or "S")	MPa	49	17	3
Material fitting parameter	$S_2 = S_4$ (or "s")	-	1	1	1
Material fitting parameter	S_3 (or "S")	MPa	8	0.8	0.36

Table 5. Summary of the structural material parameters as least-squares fitted from the results of uni-axial fatigue and tensile tests

Ductile damage component "$D_{ductile}$"
The ductile damage is calculated based on the damage evolution model introduced by Bonora-Gentile-Pirondi (2004) for a uniaxial loading case. We evaluate the strain in the "ε_x" direction (this is the circumferential or hoop direction for the CC and the lateral direction of the TMF panel) where the largest deformation is expected.

$$D_{ductile,(i+1)} = D_0 + (D_{cr} - D_0)\left\{1 - \left[1 - \frac{\ln(\varepsilon(i+1)/\varepsilon_{\mathrm{th}})}{\ln(\varepsilon_{\mathrm{f}}/\varepsilon_{\mathrm{th}})}\right]^{\alpha}\right\} \quad \text{Eq. 20}$$

as "D_0=0" for the virgin material, the equation may be written as:

$$D_{ductile,(i+1)} = D_{cr}\left\{1 - \left[1 - \frac{\ln(\varepsilon_{(i+1)}/\varepsilon_{\mathrm{th}})}{\ln(\varepsilon_{\mathrm{f}}/\varepsilon_{\mathrm{th}})}\right]^{\alpha}\right\} \quad \text{Eq. 21}$$

For the CC's copper-based alloy CuCrZr the three main temperatures, evaluated during uni-axial material tests, are considered during the post-processing fatigue life analysis: T1 = 300[K], T2= 700[K], T3 = 900[K]. Accordingly, the following temperature fields can be defined:

- "$J_{300[K]\Rightarrow 700[K]}$" for the temperature between 300[K] and 700[K];
- "$J_{700[K]\Rightarrow 900[K]}$" for the temperature between 700[K] and 900[K].

The parameters "$\varepsilon_{\mathrm{th}}$" and "$\varepsilon_{\mathrm{f}}$" are material constants at a given temperature condition and "ε" is the strain, extracted from the FE analysis. The application of the equation (Eq. 21) with the temperature fields integrated, takes the following form:

$$\begin{cases} D_{i,ductile,(300K)} = D_{cr}\left\{1 - \left[1 - \frac{\ln(\varepsilon_{(i+1)}/\varepsilon_{th})}{\ln(\varepsilon_f/\varepsilon_{th})}\right]^{\alpha}\right\} \\ \quad \downarrow J_{300\Rightarrow 700\mathrm{K}} \\ D_{i,ductile,(700K)} = D_{cr}\left\{1 - \left[1 - \frac{\ln(\varepsilon_{(i+1)}/\varepsilon_{th})}{\ln(\varepsilon_f/\varepsilon_{th})}\right]^{\alpha}\right\} \\ \quad \downarrow J_{700\,[\mathrm{K}]\Rightarrow 900\,[\mathrm{K}]} \\ D_{i,ductile,(900K)} = D_{cr}\left\{1 - \left[1 - \frac{\ln(\varepsilon_{(i+1)}/\varepsilon_{th})}{\ln(\varepsilon_f/\varepsilon_{th})}\right]^{\alpha}\right\} \end{cases} \quad \text{Eq. 22}$$

Depending on the given temperature field "$J_{300[K]\Rightarrow 700[K]}$" or "$J_{700[K]\Rightarrow 900[K]}$", as well as defined temperature "T_i" (T_i is equal to T_1= 300[K] or T_2=700[K] or T_3=900[K]), the following parameters are calculated:

$$\begin{cases} T_{i,J1} = \beta * T_1 + (1-\beta) * T_2 \\ T_{i,J2} = \beta * T_2 + (1-\beta) * T_3 \end{cases} \quad \text{Eq. 23}$$

which can be written as:

$$\begin{cases} \beta_{i,J1} = \frac{T_{i,J1} - T_2}{T_1 - T_2} \\ \beta_{i,J2} = \frac{T_{i,J1} - T_3}{T_2 - T_3} \end{cases} \quad \text{Eq. 24}$$

After the parameter "β" is calculated, the ductile damage is determined by the following linear interpolation equations:

$$\begin{cases} D_{ductile,(Ti,J1)} = \beta_{i,J1} * D_{i,ductile\,(300K)} + (1-\beta_{i,J1}) * D_{i,ductile\,(700K)} \\ D_{ductile,(Ti,J2)} = \beta_{i,J2} * D_{i,ductile\,(700K)} + (1-\beta_{i,J2}) * D_{i,ductile\,(900K)} \end{cases} \quad \text{Eq. 25}$$

Brittle damage component "$D_{brittle}$"

Zero brittle damage is assumed for the virgin state of the material:

$$D_{brittle,0}=0$$

The subsequent values of the brittle fatigue damage are determined incrementally:

$$D_{brittle,(i+1)} = D_{brittle,i} + \Delta D_{brittle,(i+1)} \quad \text{Eq. 26}$$

where, "$D_{brittle,i}$" is the value of brittle damage at the i-th converged substep of the FE analysis, and the damage increment "$\Delta D_{brittle,(i+1)}$" is calculated based on the damage rate evolution equation of Dufailly-Lemaitre (1995),:

$$\Delta D_{brittle,(i+1)} = \dot{D}_i \Delta t_i = (\frac{Y_{(i+1)}}{S})^s \dot{p}_{(t)} \Delta t_i \quad \text{Eq. 27}$$

The parameters "S" and "s" are the damage exponent material fitting parameter in dependency on a given material temperature condition (as shown in Table 5, for temperature condition of e.g. 900[K] "$S=S_1=3$", "$S=S_2=1$"). The parameter "$\dot{p}_{(t)}$" is the accumulated plastic strain rate at the given condition as extracted from the FE analysis. "Y" is the strain energy density release rate, and it is defined as:

$$Y = \frac{\sigma_{eq}^2 R_v}{2E(1-D)^2} \quad \text{Eq. 28}$$

The incremental brittle damage equation is:

$$\Delta D_{brittle,(i+1)} = \left(\frac{\sigma_{eq,i}^2 R_{v,i}}{2ES}\right)^s \dot{p}_{(t)} \Delta t_i \quad \text{Eq. 29}$$

where "R_v" is the triaxiality function:

$$R_v = \frac{2}{3}(1+\nu) + 3(1-2\nu)(\frac{\sigma_H}{\sigma_{eq}})^2 \quad \text{Eq. 30}$$

and "Δt_i" is the time increment written as:

$$\Delta t_i = t_i - t_{i-1} \quad \text{Eq. 31}$$

In contrary to the original equation (Eq. 17) by Dufailly-Lemaitre for damage rate calculation, where a value of "$(1\text{-}D)^2$" is used as a conversion factor between the effective and a classical stress, in equation (Eq. 29) the conversion factor is omitted, as a classical stress values are extracted from the FE analysis.

Finally, the following linear interpolation is used to accounting for the temperature dependency of the brittle damage:

$$\begin{cases} D_{brittle,(Ti,J1)} = \beta_{i,J1} * D_{i,brittle\,(300K)} + (1-\beta_{i,J1}) * D_{i,brittle\,(700K)} \\ D_{brittle\,,(Ti,J2)} = \beta_{i,J2} * D_{i,brittle\,(700K)} + (1-\beta_{i,J2}) * D_{i,brittle\,(900K)} \end{cases}$$

Eq. 32

Results

The CC's wall was evaluated against the critical damage "D_{cr}=0.61" at which a complete failure for the CuCrZr material occurs. Theoretically, for damage to occur, the condition of "D_{cr}=1" must be met. However, considering the void and crack interactions, the critical damage is smaller for most materials [22]. As presented in Figure 8, the damage was calculated at the critical point "node 1" – where failure is predicted due to lowest fatigue life. Furthermore, two additional points in thickness direction of the wall – up to node 3, located at the laser loaded side of the TMF panel, were evaluated. The dominant failure part is ductile damage, whereas the brittle part of the damage is found to be insignificant.

As shown in Figure 9 (combined damages), for node 3 – at the laser loaded side, where the damage evolution exponent value "α" is smaller ($\alpha \approx 0.14$) (values for damage evolution given in Table 5), a low initial damage rate is obtained which quickly expands as the failure strain is reached (Figure 10 and Figure 11). The initial slow and localized nucleation phase is followed by either a rapid void coalescence or inter-void ligament fracture. At node 1 – inside the cooling channels area, where the damage evolution exponent "α" is higher ($\alpha \approx 0.4$), the extensive void nucleation stage and coalescence occurs as a consequence of the necking of the inter-void ligament [23]. For this case, it may be noticed that the brittle failure is smaller when compared to damage at node 3 (on the laser loaded side).

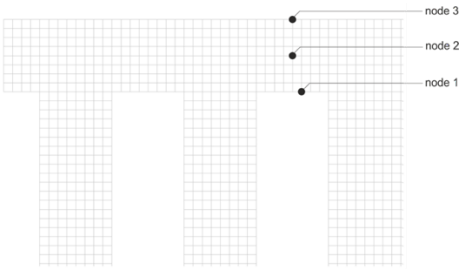

Figure 8 Cross section of the CC TMF panel with indicated nodes for fatigue life evaluation

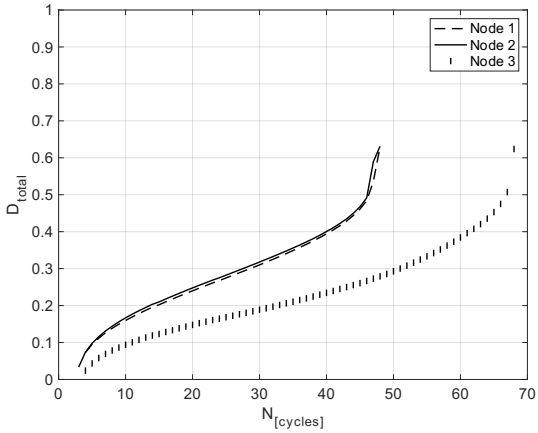

Figure 9 Combined damage at nodes 1,2,3 vs number of cycles until critical damage occurs (crack initiation)

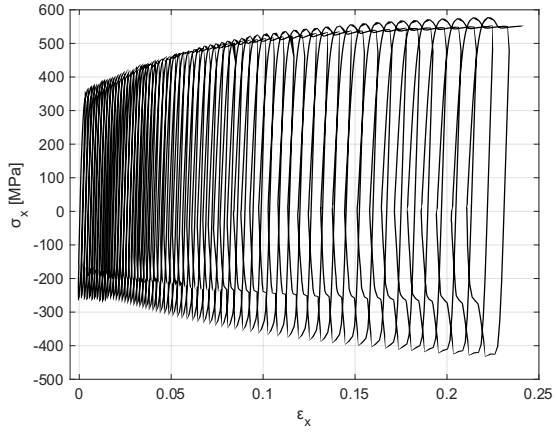

(a) Stress-strain at node 3

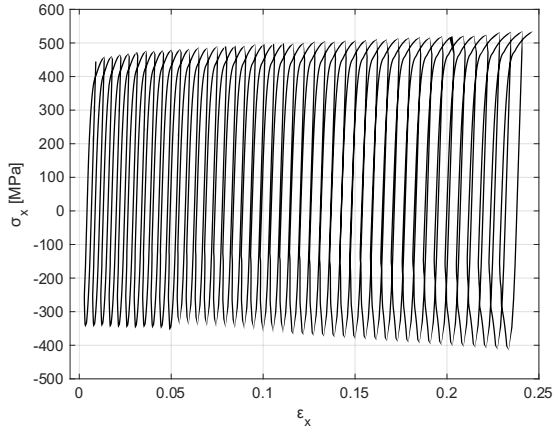

(b) Stress-strain at node 2

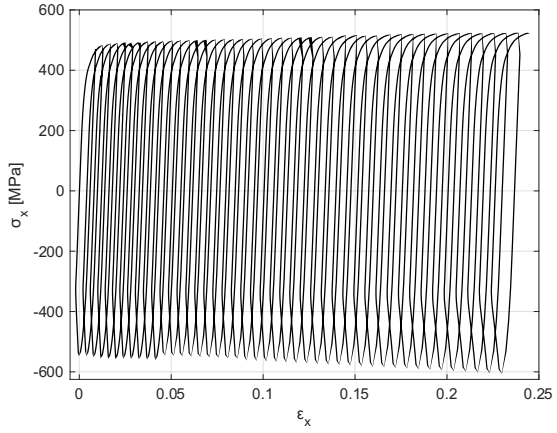

(c) Stress-strain at node 1

Figure 10 Stress-strain curves in circumferential direction at (a) node 3, (b) node 2 and (c) node 1, plotted based on the numerical analysis for all cycles until critical damage D_{cr}=0.61 is reached.

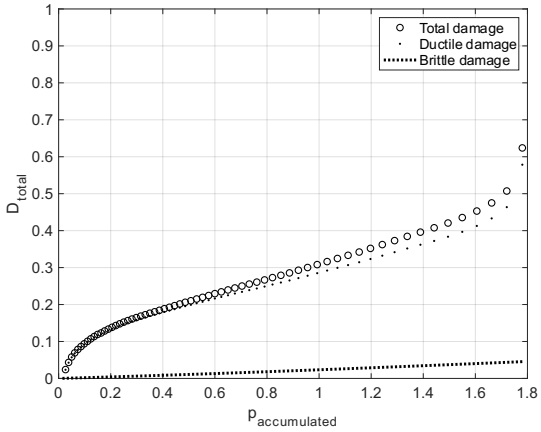

(a) Damage in dependency on the accumulated plastic strain at node 3

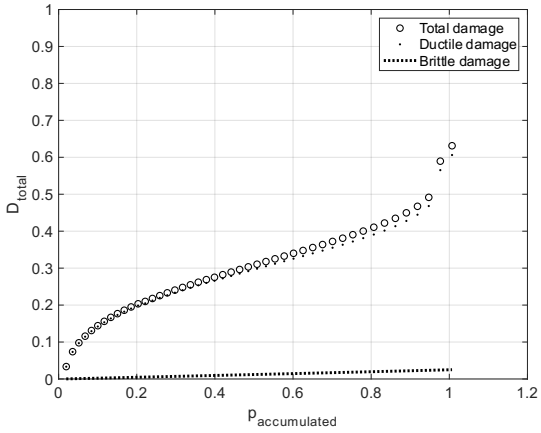

(b) Damage in dependency on the accumulated plastic strain at node 2

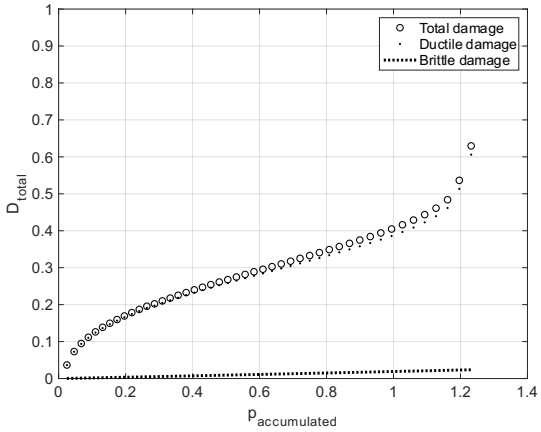

(c) Damage in dependency on the accumulated plastic strain at node 1

Figure 11 Total damage propagation (sum of ductile and brittle damage) in dependency on the accumulated plastic strain at (a) node 3, (b) node 2, (c) node 1 (failure point)

Damage evolution studies based on two initial numerically acquired cycles

As the computational cost is substantial when the slow progressive damage in the material is calculated by a FE analysis over a large number of load cycles, it is more advantages to model numerical fatigue life response of a small part of the loading history. A significant reduction of the FE analysis time and ability to quickly estimate the critical damage of the CC and number of cycles to failure is realized, by incorporating only the first two FE analysis cycles into the post processing damage-parameter based fatigue life analysis. The total damage value for cycle number 3 and its follow-on cycles is calculated by assuming the same stress-strain behaviour of the hysteresis loop as in the 2nd cycle until the critical damage is reached. The variables "$\varepsilon_{elastic,cycle(i)}$", "$\varepsilon_{plastic,cycle(i)}$" and "$\dot{p}_{(t),cycle(i)}$" are updated in accordance with equation (Eq. 33), and the remaining numerical parameters, are reused from cycle number 2 for each sub-step of cycle number 3 and higher.

$$\begin{cases} \varepsilon_{elastic,cycle(i)} = \left(\varepsilon_{elastic,cycle(i-1)} - \varepsilon_{elastic,cycle(i-2)}\right) + \varepsilon_{elastic,cycle(i-1)} \\ \varepsilon_{plastic,cycle(i)} = \left(\varepsilon_{plastic,cycle(i-1)} - \varepsilon_{plastic,cycle(i-2)}\right) + \varepsilon_{plastic,cycle(i-1)} \\ \dot{p}_{(t),cycle(i)} = \left(\dot{p}_{(t),cycle(i-1)} - \dot{p}_{(t),cycle(i-2)}\right) + \dot{p}_{(t),cycle(i-1)} \end{cases}$$

Eq. 33

In Figure 12, the combined results for node 1, 2 and 3 of the damage increase (up to a critical value at D_{cr}=0.61) in function of number of cycles was presented (shown in a similar manner as Figure 9). When comparing Figure 9 and Figure 12, it may be concluded that the post-processing calculations derived from the first two numerically obtained cycles is more conservative for node 3, whereas fatigue life prediction for nodes 1 and 2 represents a good coincidence with the post processing results where all FE cycles to failure for the CC are calculated.

The more detailed diagrams with a stress-strain curves of the initial FE obtained cycles, as well as damage in function of accumulated plastic strain, are highlighted in the following page (Figure 13 and Figure 14). A plastic shakedown behaviour can be observed for node 3, as well as a predominant ratcheting response at node 1 – these may be better observed in diagrams with only two cycles, as shown in Figure 13 and Figure 14. Presumably, at node 3, the annealed metal tends to harden in direction of the stable limit under plastic strain-controlled loading. As may be noted from Figure 10 and Figure 11 – node 3 with all cycles to failure analysed, and Figure 13 and Figure 14 – node 3 where only two cycles were analysed, the prediction of the critical damage and number of cycles to failure is less accurate where the plastic shakedown with a small "$\Delta\varepsilon$" is observed.

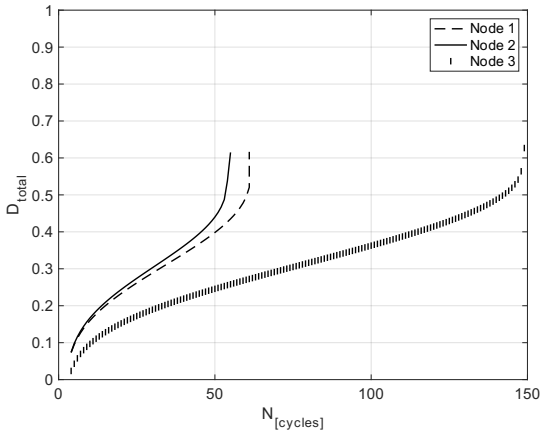

Figure 12 Combined results of nodes 1,2,3 with number of cycles until critical damage occurs, based on 2-numerically acquired cycles

As aforementioned, in the support to the post-processing method, the FE analysis of the deformation and distortion process due to thermal loading and mechanical loads arising from the pressure within the cooling channels is used. As shown in the previously presented stress-strain diagrams (Figure 10), due to large temperature driven cyclic loading, a significant deformation (leading to low cycle fatigue failure) is recorded in the CC thin wall area. The presented hysteresis loops, indicates a ratchetting behaviour, where unsymmetric cycles of stress between the limits causes progressive ratchetting in the mean stress direction (e.g. Figure 10 and Figure 13). The stress-strain curve anisotropy in tension and compression tests is well-known source of ratcheting of structures [24]. The final deformation phase preceding the failure is often under large influence by the void coalescence process that rapidly pushed the net resisting area to instability. When a damage variable is approaching the critical value D_{cr}, the mutual interactions between microvoids engage to lessen the effective resisting section [22]. The presents of cycling stress (with tensile mean stress) combined with a ratcheting strain accumulation in the tensile direction as well as thinning of the components cross-section area, may lead to a permanent failure of the CC inner wall [25].

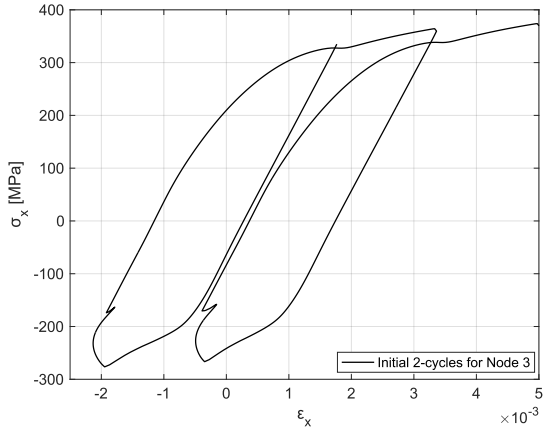

(a) Stress-strain at node 3 for cycles number 1 and 2

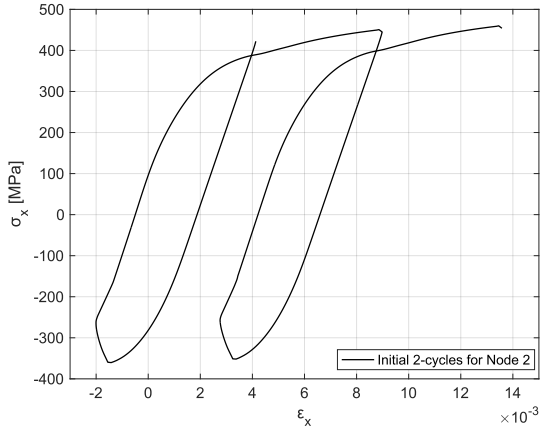

(b) Stress-strain at node 2 for cycles number 1 and 2

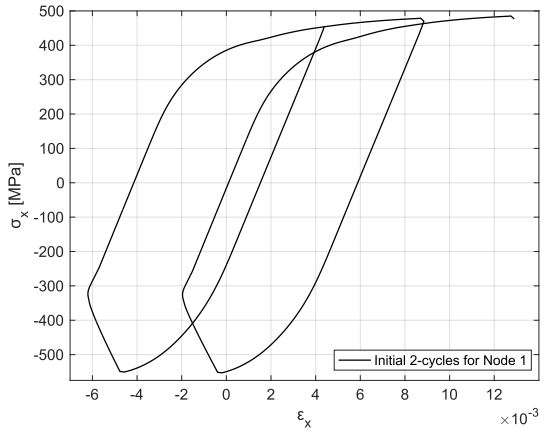

(c) Stress-strain at node 1 for cycles number 1 and 2

Figure 13 Stress-strain curves in circumferential direction at (a) node 1, (b) node 2 and (c) node 3, plotted based on the two numerical acquired cycles

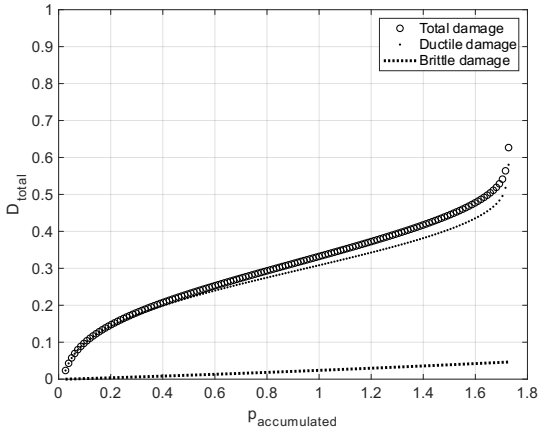

(a) Damage in dependency on the accumulated plastic strain at node 3 based on two FE analysis cycles

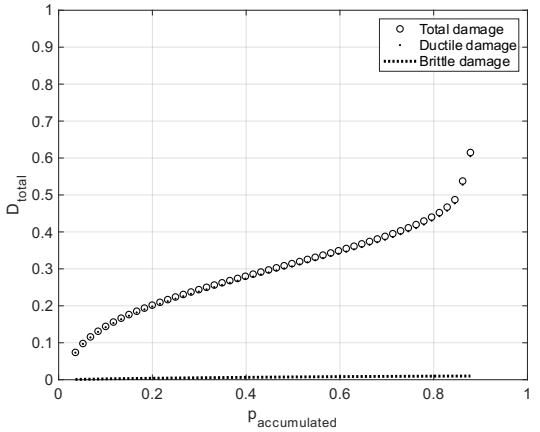

(b) Damage in dependency on the accumulated plastic strain at node 2 based on two FE analysis cycles

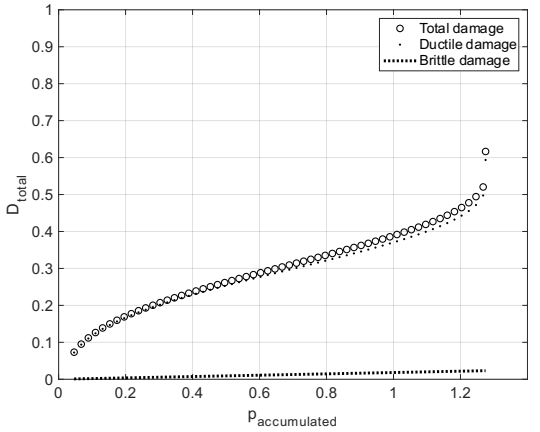

(b) Damage in dependency on the accumulated plastic strain at node 1 based on two FE analysis cycles

Figure 14 Total damage propagation (ductile and brittle damage)- accumulated plastic strain at (a) node 1 (failure point), (b) node 2, (c) node 3, based on two numerically acquired initial cycles

7. RESULTS SUMMARY AND CONCLUSIONS

A coupled thermal and structural quasi 2D Finite Element Analysis (FEA) of a CC wall nozzle throat cross-section TMF panel with a fatigue life prediction model based on damage mechanics was investigated. This model allows to efficiently simulate the damage propagation of a LRE combustion chamber suitable for reusability. The model comprises a full loading cycle with pre-cooling, start-up, hot run (due to laser loading of the TMF panel) and post-cooling. The model was validated by comparing the results with TMF panels tested at DLR Lampoldshausen. During the TMF panel test, the crack in the combustion chamber inner wall was recorded at 92 cycles for the fatigue-relevant temperature of 900[K]. Within the hereby proposed post-processing method, the calculated cycles number until crack initiation "D_{cr}=0.61" for node 1 was at 48 cycles – based on a FE analysis of all cycles to failure (Figure 9), and 52 cycles – where the calculation was based on two numerically obtained cycles (Figure 12). The calculated number of cycles to failure for node 3 – on the laser loaded side – was 70 cycles "D_{cr}=0.61" based on a FE analysis of all cycles to failure, and 148 cycles – in case where calculation was based on two numerically acquired cycles. The post-processing method, where calculations are based on the first two numerically obtained cycles is therefore more conservative and can be successfully employed in a quick estimation of the CC fatigue life for LCF analysis. The proposed approach is suitable for a quick evaluation of the remaining life of any combustion chamber of a reusable LRE. Furthermore, as highlighted in some of the previously published papers [4], [5], [7], [8], [9], [10], [26], [27], [28] the significance of adequately defined elasto-plastic material parameters for obtaining the accurate non-linear solution was presented.

The CC's inner liner was analyzed through a one-way coupled process where the damage law is introduced into this one-way coupled calculation for the highest loaded node by a post-processing of the local strain history. For the implemented method, where fatigue life analysis is based on two FE analysis cycles, this paper demonstrates that the implemented methodology provides a good coincidence of the results for the calculation of the critical number of cycles until crack initiation.

As can be observed in Figure 15 for the FE analysis, the thinning occurred in the far-left channel, whereas the failure of the TMF panel was reported in the central cooling channel. For the various tests conducted at the TMF panel test bench, the failure occurred sometimes in the different cooling channels which may be connected with a "non-ideal" fine-adjustment of the lateral position of the TMF panel in relation to the laser.

In Figure 15, the total mechanical strain in X-direction after 48cycles (circumferential or hoop direction of the CC, lateral direction of the TMF panel) is shown, where the largest deformation was obtained for the far-left cooling channel. It may be also noticed that a large deformation in X-compression is present, where the actual failure during the TMF panel tests occurs.

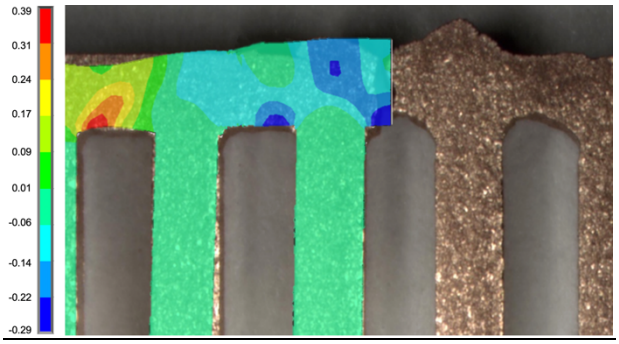

Figure 15 Cross section of the CC type TMF panel with visible deformation of the cooling channels (TMF panel test bench DLR Lampoldshausen) combined with numerical results with total mechanical strain in X-direction (circumferential or hoop direction of the CC; lateral direction of the TMF panel) after 48 cycles.

Outlook

The long-term focal point of the presented work is to mature damage propagation simulation models and to gain an in-depth understanding of the interactions between influential elements such as elevated temperature, cyclic conditions and the fatigue life mechanisms. From the results of the work presented in this manuscript, further development of the proposed methods is planned combined with a propulsion modeling activity for reusable LREs applications. The planned studies will include the evaluation of the given engine architecture supported by a system level simulation (SLS) and implementation of propulsion modeling tools, such as EcosimPro ESPSS - European Space Propulsion Simulation Toolkit. The extended research will enable for a faster and more accurate prediction of the LREs components remaining useful life for a given engine configuration.

Acknowledgement

The project leading to this manuscript has received funding from the European Union's Horizon 2020 research and innovation programme under the Marie Skłodowska-Curie grant agreement No 860956.

The project leading to this application has received funding from the European Union's Horizon 2020 research and innovation programme under the Marie Skłodowska-Curie grant agreement No 860956.

Nomenclature | Acronyms | Abbreviations

Nomenclature

α	damage evolution exponent
β	parameter calculated for temperature interpolation
γ and X_∞	kinematic hardening parameters
Δt	time increment
$\dot{\varepsilon}$	strain rate (can be also ^{e}lastic, ^{p}lastic, thermal)
ε_{th}	damage threshold strain
ε_D or ε_{th}	damage threshold strain
ε_r or ε_f	theoretical strain to failure that a ductile material would exhibit under uniaxial stress
$\dot{\varepsilon}_{ij}^{p}$	plastic strain rate second order tensor
K and N	viscosity parameters
ν	Poisson's ratio
σ_d or σ_{ij}^{D}	deviatoric stress – stress component which changes the shape of a given specimen
σ^{eff}	the stress that has to be applied to an undamaged material to cause the strain occurring in the damaged material under the nominal stress.
σ_{eq}	equivalent stress
σ_H	hydrostatic stress – stress component which changes the volume of the given specimen. An average of the three normal stress components of any stress tensor
σ_{ij}^{D}	stress deviator
σ_{kk}	stress with two identical indices kk
σ_s	actual yield stress
σ_u	ultimate stress
D	decrease of the elastic modulus $\acute{E}$ induced by damage
D_0	initial damage
D_{cr}	critical damage
$\dot{D}$	damage rate, kinetic damage
D_{total}	total damage
E_0 or E	Young's modulus where D=0, undamaged material
E_{eff} or $\widetilde{E}$	Young's modulus of a damaged material
f	yield function
$J_{x[K]\Rightarrow x[K]}$	temperature field for temp. "x"
$\dot{p}$	accumulated plastic strain rate
Q	heat flux
R_ν or $f\left(\frac{\sigma_m}{\sigma_{eq}}\right)$	triaxiality function
R_∞ and R_0	isotropic hardening or softening parameters
S an s	material fitting parameter
t	time
T	temperature
Y	damage energy release rate

Acronyms/Abbreviations

APDL	ANSYS Parametric Design Language
ASCenSIon	Advancing Space Access Capabilities Reusability and Multiple Satellite Injection
CC	Combustion Chamber
CDM	Continuum Damage Mechanics
ESPSS	European Space Propulsion Simulation Toolkit
FEA	Finite Element Analysis
FEM	Finite Element Method
HCF	High Cycle Fatigue
LCF	Low Cycle Fatigue
LCH4	Liquid Methane
LOx	Liquid Oxygen
LREs	Liquid Rocket Engines
MLC	Main Life Cycle
NASA	National Aeronautics and Space Administration
Prometheus	Precursor Reusable Oxygen Methane cost Effective propulsion System
RLV	Reusable Launch Vehicle
RVE	Reference Volume Element
Solid185	Eight nodes having three degrees of freedom at each node
SLS	System Level Simulation
STD	Standard
TMF	Thermo-Mechanical Fatigue
VLCF	Very Low Cycle Fatigue

8. REFERENCES

[1] S. Stappert, J. Wilken, L. Bussler, and M. Sippel, "A systematic assessment and comparison of reusable first stage return options," *Proc. Int. Astronaut. Congr. IAC*, vol. 2019-Octob, pp. 1–15, 2019.

[2] M. T. Gulczynski *et al.*, "RLV applications: challenges and benefits of novel technologies for sustainable main stages," Oct. 2021. [Online]. Available: https://elib.dlr.de/148758/

[3] A. Iannetti, N. Girard, C. Bonhomme, N. Ravier, E. Edeline, and F. De Vernon, "PROMETHEUS, A LOX/LCH4 REUSABLE ROCKET ENGINE," *7th Eur. Conf. Aeronaut. Sp. Sci.*, no. EUCASS 2017-537, pp. 1–9, 2017, doi: 10.13009/EUCASS2017-537.

[4] J. R. Riccius, E. B. Zametaev, W. Bouajila, and Q. Wargnier, "Inner liner temperature variation caused deformation localization effects in a multichannel model of a generic LRE wall structure," *50th AIAA/ASME/SAE/ASEE Jt. Propuls. Conf. 2014*, pp. 1–12, 2014, doi: 10.2514/6.2014-3988.

[5] R. G. Thiede, J. R. Riccius, and S. Reese, “Life prediction of rocket combustion-chamber-type thermomechanical fatigue panels,” *J. Propuls. Power*, vol. 33, no. 6, pp. 1529–1542, 2017, doi: 10.2514/1.B36361.

[6] N. T. Standard, “NASA-STD-5012B STRENGTH AND LIFE ASSESSMENT REQUIREMENTS FOR LIQUID-FUELED SPACE PROPULSION SYSTEM ENGINES.” 2016.

[7] W. Zhang, *Failure characteristics analysis and fault diagnosis for liquid rocket engines*. 2016.

[8] R. Strunz and J. W. Herrmann, “Reliability as an independent variable applied to liquid rocket engine test plans,” *J. Propuls. Power*, vol. 27, no. 5, pp. 1032–1044, 2011, doi: 10.2514/1.B34279.

[9] J. S. Hardi *et al.*, “High frequency combustion instabilities in liquid propellant rocket engines : research programme at DLR Lampoldshausen,” *Proc. Int. Symp. Thermoacoustic Instab. Ind. meets Acad.*, no. January, pp. 1–11, 2016.

[10] A. Babu, A. . Asraff, and N. Philip, “Fatigue Life Prediction of a Rocket Combustion Chamber,” *IOSR J. Mech. Civ. Eng.*, vol. 11, no. 5, pp. 12–20, 2014.

[11] R. B. Hetnarski, *Encyclopedia of Thermal Stresses*. 2014.

[12] A. Babu, A. . Asraff, and N. Philip, “Fatigue Life Prediction of a Rocket Combustion Chamber,” *IOSR J. Mech. Civ. Eng.*, vol. 11, no. 5, pp. 12–20, 2014, doi: 10.9790/1684-11521220.

[13] V. Buljak and G. Ranzi, *Constitutive Modeling of Engineering Materials*, 1st Editio.

[14] P. O. Bouchard, L. Bourgeon, S. Fayolle, and K. Mocellin, “An enhanced Lemaitre model formulation for materials processing damage computation,” *Int. J. Mater. Form.*, vol. 4, no. 3, pp. 299–315, 2011, doi: 10.1007/s12289-010-0996-5.

[15] N. Bonora, D. Gentile, and A. Pirondi, “Identification of the parameters of a non-linear continuum damage mechanics model for ductile failure in metals,” *J. Strain Anal. Eng. Des.*, vol. 39, no. 6, pp. 639–651, 2004, doi: 10.1243/0309324042379356.

[16] X. Zhang, Z. Chen, and Y. Liu, “Constitutive Models,” 2017, pp. 175–219. doi: 10.1016/B978-0-12-407716-4.00006-5.

[17] J. Dufailly and J. Lemaitre, “Modeling Very Low Cycle Fatigue,” *International Journal of Damage Mechanics*, vol. 4, no. 2. pp. 153–170, 1995. doi: 10.1177/105678959500400204.

[18] G. Waxenegger-Wilfing, K. Dresia, J. C. Deeken, and M. Oschwald, “Heat transfer prediction for methane in regenerative cooling channels with neural networks,” *J. Thermophys. Heat Transf.*, vol. 34, no. 2, pp. 347–357, 2020, doi: 10.2514/1.T5865.

[19] J. Deeken, D. Suslov, O. Haidn, and S. Schlechtriem, “Combustion efficiency of a porous injector during throttling of a LOx/H2 combustion chamber,” vol. 2, pp. 251–264, 2011, doi: 10.1051/eucass/201102251.

[20] P. H. KRINGE, J. R. RICCUS, and M. OSCHWALD, “LOW-COST LIFE ASSESSMENT OF LIQUID ROCKET ENGINES by replacing full-scale engine tests with TMF panel tests,” vol. 73, pp. 154–162, 2020.

[21] M. Oschwald *et al.*, “Measurement of Heat Transfer in Liquid Rocket Combustors,” 2020, pp. 281–331. doi: 10.2514/5.9781624105814.0281.0332.

[22] N. Bonora, “A NONLINEAR CDM MODEL FOR DUCTILE FAILURE,” 1997.

[23] U. Sarajärvi and O. Cronvall, *A Procedure to Generate Input Data of Cyclic Softening and Hardening for FEM Analysis from Constant Strain Amplitude Fatigue Tests in LCF Regime*, no. March. 2007.

[24] H. Mahbadi and M. R. Eslami, “Cyclic loading of thick vessels based on the Prager and Armstrong-Frederick kinematic hardening models,” *Int. J. Press. Vessel. Pip.*, vol. 83, no. 6, pp. 409–419, 2006, doi: 10.1016/j.ijpvp.2006.02.031.

[25] S. K. Paul, “A critical review of experimental aspects in ratcheting fatigue: microstructure to specimen to component,” *J. Mater. Res. Technol.*, vol. 8, no. 5, pp. 4894–4914, 2019, doi: 10.1016/j.jmrt.2019.06.014.

[26] G. Waxenegger, J. Riccius, E. Zametaev, J. Deeken, and J. Sand, “Implications of Cycle Variants, Propellant Combinations and Operating Regimes on Fatigue Life Expectancies of Liquid Rocket Engines,” 2017.

[27] T. Masuoka and J. R. Riccius, “Life evaluation of a combustion chamber by thermomechanical fatigue panel tests based on a creep fatigue and ductile damage model,” *Int. J. Damage Mech.*, vol. 29, no. 2, pp. 226–245, 2020.

[28] K. Dresia, G. Waxenegger-Wilfing, J. Riccius, J. Deeken, and M. Oschwald, “Numerically Efficient Fatigue Life Prediction of Rocket Combustion Chambers Numerically E ffi cient Fatigue Life Prediction of Rocket Combustion Chambers using Artificial Neural Networks,” *Eucass*, 2019, doi: 10.13009/EUCASS2019-264.